Appendix: Reading of Mann wind fields in the aeroelastic codes

The Mann model includes uniform wind shear. The uniform, linear wind shear results in eddies first arriving at a higher vertical location and then at lower vertical location (z_a and z_b in Figure 27, respectively). Eddies first arriving at higher vertical locations has been observed in nature and LES[47]. As seen in figure 28, the pre-processed 11.4 m/s Mann wind field generated using the IEC turbulence simulator for the Offshore Code Comparsion Collaboration (OC3)[48] also demonstrates turbulent eddies being stretched from lower z and x to higher z and x. Assuming Taylor's hypothesis of frozen turbulence is valid, then the spatial and temporal domains can be related such that $t = x/\bar{u}$ and $k_1 = 2\pi f/\bar{u}$. Therefore, Figures 27 and 28 are in agreement assuming the wind propagation direction in both figures is from the left to the right. In other words, a wind turbine at the right of Figure 28 should first see the YZ slice at $x = 7980$ m and then from $x \approx 7979$ m and so on.

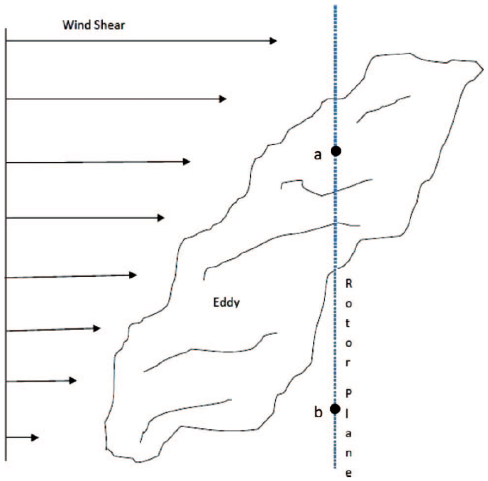

FIGURE 27 Eddy schematic. Image from Chougule et al.[47].

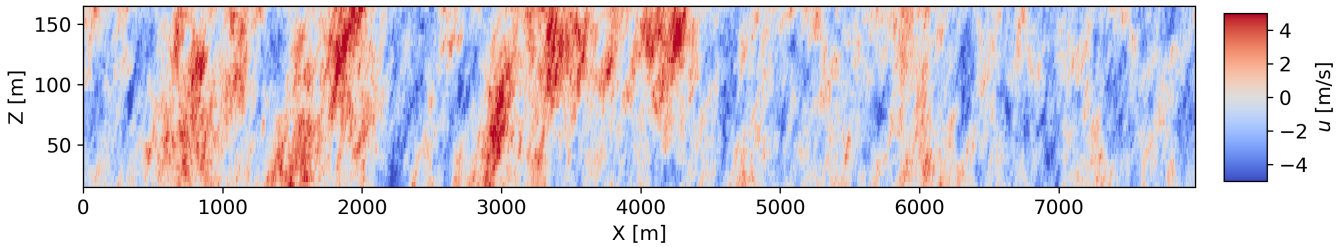

FIGURE 28 Raw Mann wind field.

However, the pre-processed wind field shown in Figure 28 is not equivalent to the wind field seen in by wind turbines in many aeroelastic codes. Based on many code-to-code comparisons (OC3, for example), HAWC2, FAST, FAST.Farm, SIMA, and other aeroelastic codes all read the Mann wind in the same way. The aeroelastic codes read the wind fields with increasing x, i.e., the wind turbine is on the left of Figure 28 and wind propagates from the right to the left, resulting in turbulent eddies arriving first at lower z. This phenomenon can be described mathematically by calculating the phases ϕ between two vertically separated time series i and j. The phase can be calculated from the complex cross-spectra $C_{i,j}$:

$$C_{i,j}(f, \Delta Z) = \hat{u}_i(f, z_a)\hat{u}_j^*(f, z_b) \tag{11}$$

$$\phi_{i,j}(f, \Delta Z) = \arg(C_{i,j}(f, \Delta Z)) \tag{12}$$

where f is frequency, $\Delta Z = z_a - z_b$, $\hat{u}_i(f, z_a)$ is the complex-valued Fourier transform of the ith velocity component $u_i(t)$ at height z_a and * denotes complex conjugate.

The OC3 wind field was fed through OpenFAST v0.1.0 and time series of the wind field velocity components at $z_{hub} = 90$ m and $z_{hub} + \Delta z = 94.6875$ m were obtained. The phases calculated in Figure 29 show that time series at $z_{hub} + \Delta z$ lag compared to z_{hub} for all three velocity components. This can also be observed qualitatively by looking at the time series in Figure 29.

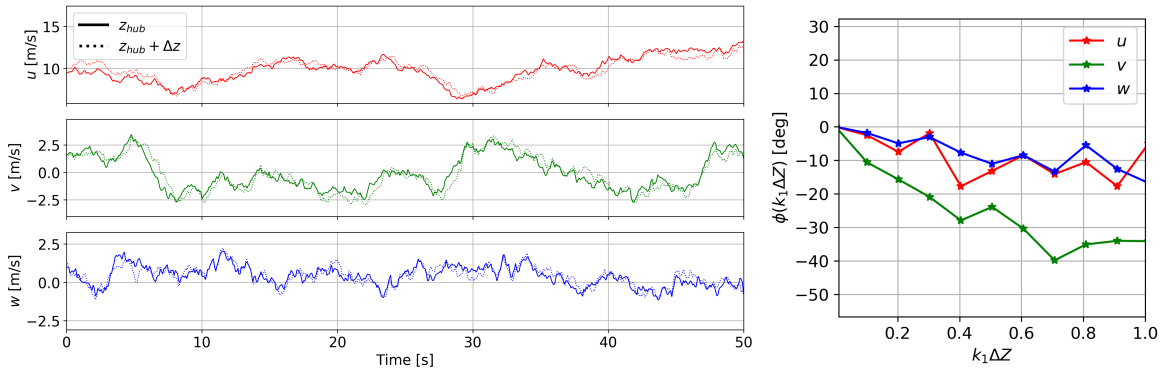

FIGURE 29 Time series (left) and spectral phases (right) for all three velocity components of the OC3 wind. Outputs are from OpenFAST v0.1.0.

Figure 29 reveals that the phase lag is most obvious in the v-velocity component. Lateral velocity component (unmodified, official version) FAST.Farm vtk outputs for Mann wind and wind generated from an LES precursor for the same wind speed, turbulence, and shear exponent are compared in Figure 30. It is clear that the eddies are stretched in opposite direction for Mann compared to LES (wind propogation is in the positive x-direction). In the present work, FAST.Farm and OpenFAST are modified to read the files in the opposite direction compared to the official versions to correct this apparent error.

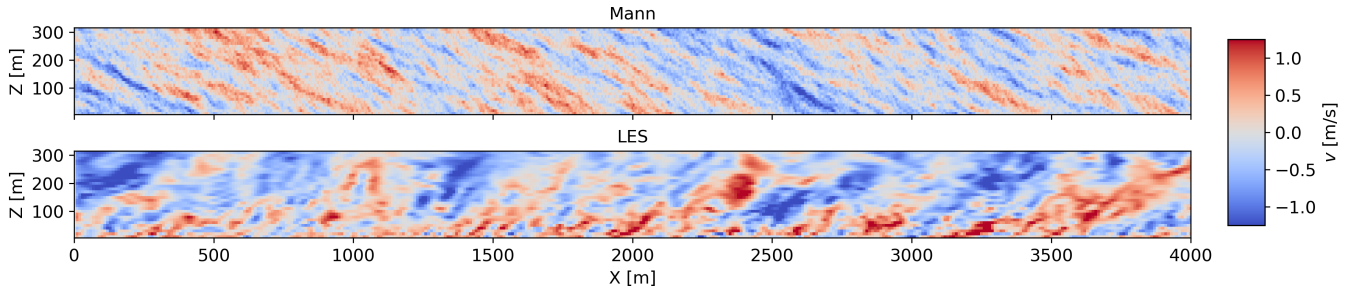

FIGURE 30 Lateral velocity component FAST.Farm outputs for Mann wind and wind generated from an LES precursor (neutral atmospheric stability, 8 m/s, 10 % TI case in Jonkman et al.[14])

How to cite this article: A. Wise and E. Bachynski (2019), Wake meandering effects on floating wind turbines, *Wind Energy*, *2019;00:1–6*.